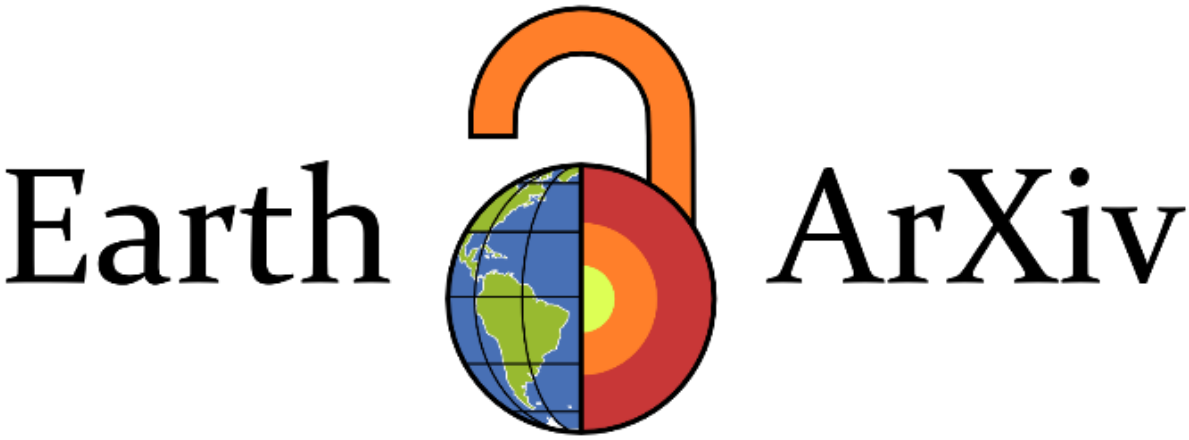

Less is more: how to capture carbon efficiently – lessons from long-term rock weathering and soil development in natural warm temperate ecosystems.

Dimitar Z. Epihov[1]

[1] *Plants, Photosynthesis and Soil cluster, School of Biosciences, University of Sheffield, Western Bank, S10 2TN, UK*

Abstract

Enhanced rock weathering (ERW) has been proposed as a viable strategy to offset greenhouse gas emissions. The field is currently plagued by uncertainty in the rates of C capture through alkalinity export, resulting from variation in extent and lag due to soil exchange, secondary minerals, and effects on soil organic carbon. Provided are quantitative estimates for weathering losses in these pools using a natural weathering system on a volcanic rock hill, Bulgaria. Two distinct soils are compared: mafic soils derived predominantly from cation-rich basalt (81–85%) with minor dacite (~15–19%), and felsic soils (66% dacite, 34% basalt). Major cations were partitioned into four pools: primary minerals, exchangers, clays, and leached. Leaching accounted for 34% of total cations in felsic soils and 12% in mafic soils. Exchangers and clays accounted for ~50% of all cations in felsic soils compared to 25% in mafic soils. Only 16% of cations remained in primary minerals in felsic soils versus 62% in mafic soils. Goethite peaked in felsic soils and correlated with ~2-fold larger soil organic carbon stocks than in mafic soils. These findings suggest that CO_2 removal potential in ERW may be overestimated, and that smaller basalt applications may more rapidly boost inorganic and organic C capture.

Introduction

The processes of physical comminution and chemical dissolution of geological parent material, collectively termed rock weathering, drive the formation of soils over millenia [1]. Soon after rock weathering commences, colonisation by biological systems including microbial life, lower plants and ultimately more complex grassland and woodland communities act as biotic factors further shaping the soil formation (pedogenesis) process [2].

Biotic factors can simultaneously accelerate [3] and decelerate [4] rock weathering, prompt the transformation of certain clay phases [5], and lead to the accumulation of soil organic matter (SOM)[6]. Belowground respiration – including both plant root respiration (autotrophic) and microbial respiration (heterotrophic) – increases the soil concentration of CO_2 over and above the levels reached through simple atmosphere-soil equilibration as dictated by Henry's law. As a result of this *biotic CO_2 concentrating pump*, levels of 10,000-60,000

ppm CO_2 are commonplace in the soil atmosphere [7], making the soil solution enriched in carbonic acid (H_2CO_3) and rendering it weakly acidic. These acidic soil solutions react with rock minerals promoting the release of base cations and alkalinity [8] as per the equation illustrating the dissolution of the common rock-forming pyroxene mineral diopside (Eq.1):

$$\underset{diopside}{CaMgSi_2O_6} + \underbrace{4CO_2 + 6H_2O}_{carbonic\ acid} \rightarrow Ca^{2+} + Mg^{2+} + 4HCO_3^- + 2H_4SiO_4 \qquad Eq.1$$

Thus, rock weathering actively promotes carbon dioxide removal ($CDR_{weathering}$) from the atmosphere, realzing its storage either in water-dissolved bicarbonate/carbonate anionic form or solid form through the formation of sedimentary carbonate rocks at the bottom of the ocean [9].

Enhanced rock weathering (ERW) represents a novel approach to fight climate change by increasing $CDR_{weathering}$ through the addition of ground volcanic rock to topsoils of agricultural land [10]. Although research suggests its wide scale application can deliver C capture on gigatonne scales [11], the efficacy of weathering in human time-scales and its utility to meet climate targets, is frequently questioned [12],[13]. In no small part, lags as those stated, $WR\text{-}lag_{biomass}$ and $WR\text{-}lag_{exchange}$ play a role in limiting the annual fluxes of alkalinity in soils amended with volcanic dust [14]. Furthermore, the increases in soil pH and nutrient improvement brought about by rock weathering [10] can augment soil microbial activity leading to destabilization, at least temporally, to soil organic carbon (SOC) stocks, degassing CO_2 back to the atmosphere [15]. Moreover, the increases in the soil concentration of divalent cations caused by rock weathering can promote the transformation of clay minerals driving the isomorphic substitution and fixation of weathering cations into the clay lattice [16]. As clays are generally subject to slow weathering kinetics this imposes another lag in alkalinity export ($WR\text{-}lag_{clays}$).

It is clear that uncertainties in the timescales of these lags and the rock weathering-SOC interactions require further investigation. However, research into these is complicated not at the least because of the novelty of the ERW technology and the lack of decadal field trials. For instance, the current longest-running ERW field trial (Energy Farm, US) only just turned 8-years since its first basalt rock dust application [10]. Some of these knowledge gaps can be bridged by geochemical modelling [11] but the role of biology and biotic factors, controlling many of these lags, is hard to incorporate comprehensively into existing models. An obvious solution, allowing the researcher the ability to 'time-travel' in order to provide an empirical framework to some of these lags could be provided by the use of chronosequences of natural volcanic rocks. This tool, widely adopted by ecologists [17],[18] soil scientists [19], and geochemists [20], utilises systems of rock substrates/soils/communities of different ages to provide useful insights into the long-term fate of processes that operate on medium-to long-term geological timescales. In view of ERW, studying natural volcanic landscapes of a few-thousand-years age can provide key information on weathering kinetics and lags in $CDR_{weathering}$ as these ecosystems represent the cumulative millenial effects of biotic and abiotic

factors. Moreover, studying soil chronosequences developed on volcanic rocks, particularly from the perspectives of C capture, would likely provide fresh insights into unrealized C sequestration pathways, thus paving the way for novel biogeochemical solutions for climate change mitigation.

Here, we utilise a sere, a sequence of communities representing distinct stages of ecological succession. These include: (a) bare ground (mosses, lichens, sparse grasses), (b) grassland (thick layers of short grasses), and (c) woodland (oak and hornbeam), developed on a volcanic hill with soils derived from the same volcanic parent material (**Figure 1a,b**). The sere located on the basaltic volcanic hill of Chatala in Northern Bulgaria encapsulates the processes of rock weathering and pedogenesis resulting in the formation of young 15-30 cm deep soils (**Figure 1a,b**)[21],[22]. As a rough guideline, using average soil formation rates of ~0.094 mm yr^{-1} [23], these soil depths equate to approximately 1.6-3.2 thousand years of soil development.

We characterize the inorganic and organic chemistry and mineralogy of the parent material rocks and the soils resulting from their weathering using a series of spectral and wet chemical methods. We summarise our findings on the cumulative total C removal delivered by these ecosystems and functionally separate it into realized $CDR_{weathering\text{-}alkalinity}$ and CDR_{SOC}. We also provide the first comprehensive account on the long-term fate of major cations not contributing to leached alkalinity and thus retained in the system in the context of CDR. To do that we supply figures for major cations adsorbed onto soil exchangers (short-term retention pool), major cations incorporated into clay formation (long-term retention pool), and major cations still in unweathered/partially-weathered primary minerals (medium/long-term retention pool). These allowed us to estimate the respective as-of-yet unrealized C capture potential that these retention pools have incurred. Finally, we discuss the role of parent material and biological processes in determining lags, saturation kinetics and delivering the most optimal C removal, thus directly informing current and future ERW efforts.

Results

Characterisation of parent materials

We collected a total of nine rock samples from exposed rock facies from the Chatala volcanic hill. Combined Attenuated Total Reflectance Fourier Transform Infrared (ATR-FTIR) and X-ray fluorescence (XRF) spectral analyses of the powderized rock samples revealed the presence of three distinct rock types – 6 samples were identified as basalts, 2 were classified as basaltic andesites and 1 was classified as dacite (**Figure 1c,d**). In line with these, SiO_2 and K_2O content increased from the mafic (basalts and basaltic andesites) to felsic (dacites) rocks, while the content of Mg, Fe, and Ca exhibited the opposite trend. In agreement with the differences in elemental compositions, each rock type represented distinct differences in their collected ATR-FTIR spectra (**Figure 1c**). Common rock-forming minerals and their individual FTIR spectra were compared against the average rock spectra (**Figure 1c**). Basalts and basaltic andesites contained major peaks matching major peaks in olivine, augite, and plagioclase. In contrast, dacites had no identifiable peaks for olivine and augite, but exhibited peaks traced to these of quartz.

These findings are in line with previous petrographic research at this site identifying olivine, augite, and plagioclase as the main phases of the basaltic rocks [21],[24]. To harness the full potential of the collected FTIR spectra and generate a more quantitative mineralogical analysis one needs externally validated compositions for establishing reliable calibration. To do that, we performed X-ray diffraction (XRD) spectroscopy analyses of one basalt and one dacite rock sample together with 4 soils from our sites. The resulting XRD results revealed the mineralogical composition at our site supplying a list of component minerals. The list was further used to generate over 20,000 discrete synthetic spectra based on variable contributions in component minerals and their individual FTIR spectra (**Supplementary Figure 1**). Next, we generated a partial least square (PLS) model that we validated against the XRD results (**Figure 2a; Supplementary Figure 2**). Generally, our FTIR-PLS model showed high degree of correlation with XRD measurements with most individual mineral predictions falling in the range of Pearson's $r \geq 0.8$-0.9 (except K-feldspar which was poorly predicted). Our results (**Figure 2b**) indicate that the mafic basalts and basaltic andesites lacked quartz and were low on volcanic glass (~8%) but contained high levels of the pyroxene augite (27-37%), olivine (23-24%), and more minor presence of plagioclase feldspars (2-10%). In contrast, the felsic dacites (**Figure 2b**) lacked olivine and contained lower amounts of augite (5%) but exhibited higher average content of plagioclase (19%), quartz (15%), and volcanic glass (28%). These results agree with geochemical theory of rock mineral composition [25],[26] and closely match the elemental composition patterns in **Figure 1d**.

Due to the large overlap in elemental (**Figure 1d**) and mineralogical (**Figure 2b**) composition between basalts and basaltic andesites, the mixed assemblage of extrusive igneous rocks acting as parent materials at our site could be simplified to two parent end-members – basalt and dacite.

Characterisation of soils

We collected 0-10 cm soil cores from all three seral stages (**Figure 1a,b**) including bare ground ($n = 3$ cores), grassland ($n = 3$), and woodland ($n = 6$). The FTIR spectra of sieved and crushed soil powders were also collected and used to determine their mineralogical content using the XRD-validated FTIR-PLS model. Summary of our findings (**Figure 2b**) revealed that all soils contained traces of quartz suggesting mixed parentage, i.e. soils were derived from both the quartz-less basalts and the quartz-rich dacites. Moreover, three of the woodland soil cores revealed greater quartz content (mean = 11.2%) compared to the rest of the samples (mean = 0.9%) suggesting greater contribution from dacitic parent material. In further confirmation of this view, our performed XRF analyses of soil powders revealed greater SiO_2 content, lower content of bases, and lower total Ti concentrations in these high quartz soils (**Figure 3a**). Together these results indicate that the soils under bare ground, grasslands, and quartz-poor woodlands were derived predominantly from basalt with dacite acting as an accessory parent material (mafic soils predominantly derived from the mafic basalt a minor contribution of the felsic dacite). In contrast, the three quartz-rich woodland soil cores were derived from the

weathering of dacite as a predominant parent material and basalt acting as an accessory (felsic soils).

Next, in order to calculate the quantitative contribution of each parent material to the derived soil core, we used the ratio of Al to Ti as both of these elements are relatively immobile during dissolution and their ratio should therefore remain constant throughout the weathering process (**Figure 3b**). Using a two-source mixing model, we calculated that the mafic soils including bare ground, grassland, and woodland on basalt/dacite soils were derived from 81-85% basalt with an accessory 15-19% dacite contribution (**Figure 3c**). In contrast, the felsic soils of woodland on dacite/basalt showed 66% contribution by dacite and 34% basalt (**Figure 3c**).

Soils from all four groups have relatively high pH values showing that the systems are still well buffered (**Figure 3a**), further supported by high base saturation 97.7-99.8% of soil effective cation exchange capacity (eCEC). The soil eCEC values recorded in our soils are similarly high (**Figure 3a**) as expected in a system in which the weathering of volcanic rock materials resulted in the abundant formation of trioctahedral smectitic clays (CEC 80-130 $cmol^{+}\ kg^{-1}$ [27]) and illite-smectite mixed layer clays (assuming 70-30 ratio, ~50 $cmol^{+}\ kg^{-1}$ [27]) as shown in **Figure 2b**.

The large saturation of bases on the soil exchangers together with the pronounced formation of smectitic clays point to a large retention of major cations in our system limiting alkalinity leaching and thus realized CDR.

Weathering estimates through changes in major cation budgets across parent materials and seral stages

To calculate the amount of loss in major cations through leaching, we estimated the initial baseline values of cationic stocks in our four systems. To do that we assumed a two-source mixed model from the established parent material contributions (**Figure 2c**) and their respective elemental concentrations (**Figure 1d**). Next, we compared the initial baseline concentrations to these observed in the current soils (**Figure 4a-c**). We find that all four systems have exhibited significant decline in calcium (Ca) concentrations, with mafic soils showing 20-24% decrease from initial Ca and felsic soils revealing a ~38% drop from their initial Ca levels (**Figure 4a**). Magnesium (Mg) concentrations did not significantly decrease and remained stable in mafic soils with only felsic soils exhibiting a significant decrease in Mg concentrations of approximately 18% (**Figure 4b**). Potassium (K) levels exhibited a relative increase in concentrations in all four soil systems (**Figure 4c**). These findings indicate the pronounced retention of Mg and K in Mg-rich clay phases and K-rich clay phases, respectively, which agrees with the prolific formation of Mg-rich saponites and K-rich illite-smectite in our system (**Figure 2a**). In fact, gradual Mg leaching and K fixation into the interlayers spaces may lead to the conversion of saponites to mixed layer illite-smectites over time. Our data support this view as ratios of saponite:illite-smectite drop along the seral stages (e.g., from 6:1

saponite:illite-smectite in bare soil systems to 2.4:1 ratio in mafic woodlands and 1:1 ratio in felsic woodland soils – **Figure 2a**).

Next, we estimated the absolute stocks of major cations by taking the following assumptions. We assumed that the current stocks of soil (bulk density 1.6 t m^{-3}, 50% solids) [22] according to their depth have been formed from equivalent rates of parent rock material. Thus, 15 cm and 30 cm deep soils as found in our system (**Figure 1b**) currently present ~1200 t and ~2400 t of solid soil material and would have formed from equivalent amounts of rock (1:1). We note that this is a conservative measure of weathering and thus our alkalinity losses may represent the lower end of possible CDR gained through leached alkalinity. Noting the inherent difference between soil and rock bulk density (~2.7 t m^{-3})[28], these figures would have required 4.4 cm and 8.8 cm of rock to have converted to 15 cm and 30 cm of soil, respectively. These assumptions, although simple and conservative, allowed us to produce estimated rates of $CDR_{weathering\text{-}alkalinity}$ as well as to provide empirical figures to major cation stocks held onto soil exchangers or incorporated into the structure of secondary clays. Importantly, the relationship in the pattern of distribution of cations across these 4 pools – realized CDR as leached alkalinity as well as unrealized CDR in the form of soil exchangers, clays, and unweathered material – remains unchanged by our assumptions as they only affect the absolute values.

$CDR_{weathering\text{-}alkalinity}$ was lost primarily in the form of leached Ca (**Figure 4a**), with Mg only contributing to cation losses in the felsic soil group (**Figure 4b**). We observe 10% losses of major cations from the bare ground and grassland soil systems, ~13% in the mafic woodland soil system, and approximately 34% from the felsic woodland soils (**Figure 4e**).

In order to numerically constrain the cations retained on soil exchangers, we performed exchangeable leaches of soils at their normative pH that revealed that exchanged cation pools were mainly dominated by Ca at levels at mean of 7,768 mg kg^{-1} (5,875 mg kg^{-1} in bare ground to 8,846 mg kg^{-1} in mafic woodlands), followed by K at mean of 1,235 mg kg^{-1} (878 mg kg^{-1} in bare ground soils to 1686 mg kg^{-1} in mafic woodlands), and finally Mg at mean of 1,000 mg kg^{-1} (817 mg kg^{-1} in felsic woodland soils to 1,172 mg kg^{-1} in mafic woodland soils). Thus, soil exchangers retained a minor 5 to 10% of major cations-based CDR equivalents in the system (**Figure 4e**).

Next, we determined the chemical composition of clays in our system. To do that, we collected saponite clay samples from the surface layer of altered rock gravel and subjected them to XRF analyses with final chemistry (**Figure 4d**) obtained after accounting for the measured exchangeable cations (**Figure 4d**) by subtraction. The chemical make-up of illite-smectites was determined by XRD-informed subtraction from bulk samples assuming idealized stoichiometric chemical composition for all mineral members (except for saponite which was generated as described). Our analyses of the saponites in our systems indicated concentrations of ~25,000 mg kg^{-1} Mg, ~27,000 mg kg^{-1} K, and ~18,000 mg kg^{-1} Ca – values similar to these obtained for saponite clays at European locations of similarly warm climate [29]. The Chatala saponite clays exhibited a high content of iron, Fe (~98,000 mg kg^{-1}) suggesting that they may be intermediate along the saponites-ferrosaponite end-members [30]. The illite-smectite mixed

layer clays in the Chatala system revealed lower Mg, Ca, and Fe than the saponite clays but higher K content in line with the fixation of K in illite interlayers [31] (**Figure 4d**). Using the derived clay chemical compositions and the abundance of clays in each soil group we calculated the extent of base cations (Ca, Mg, K) structurally incorporated into the clay lattice. We find that clays, counting towards unrealized CDR, amounted to 18% in mafic and 37% in felsic soils of all major cations (**Figure 4e**).

Finally, we calculated the pool of major cations in still unweathered/partially weathered primary minerals by subtracting from the total soil levels the amounts assigned to the exchangeable and clay fractions. These figures suggest that primary minerals still held onto 67%, 66%, and 62% of major cations in the mafic bare ground, grassland, and woodland soils, respectively, while only 18% in the felsic woodland system (**Figure 4e**).

Taken together our results strongly suggest that more advanced weathering stages are reached in the felsic woodland system relative to the mafic woodland system likely resulting from faster weathering of the smaller basaltic feedstock in felsic soils relative to the much larger basalt feedstock in mafic soils weathering more slowly. Evidence for this are the greater cationic stocks in secondary pools (exchangeable and clays) and greater cationic stock lost to leaching relative to the cationic stocks still in primary minerals in the felsic systems.

Iron partitioning during weathering and the formation of mineral-associated organic matter

Weathering advancement in soils is typically associated with a shift in the forms of iron (Fe) [32],[33]. At one extreme, very young primitive soils contain most of their Fe in primary mineral form (silicate-bound, magnetite-bound). At the other extreme, mature very weathered soils have most of their iron in the form of secondary oxyhydroxides. At the Chatala volcanic hill system, bare ground soils, the youngest and least developed soils, have an almost equal split of Fe in the following three pools – magnetite-bound, primary silicate-bound (e.g., olivine, augite), and secondary silicate-bound (e.g., saponite clays). Moving along the seral stages through grasslands to woodlands, the amount of secondary oxyhydroxide-bound Fe (e.g., goethite) increases at the expense of the further weathering of primary silicate-bound Fe (**Figure 5a**). Apparent is the relative immobility of Fe, as all four systems have levels broadly similar to their baselines (**Figure 5a**), with iron only transferred from one pool to another. The highest levels of secondary oxyhydroxide-bound Fe are found in the felsic woodland system exhibiting >2-fold greater concentrations of this form relative to their mafic woodland counterparts. This is consistent with the more advanced stages of weathering reached by the felsic system as previously outlined. It is worth noting that our approach behind the results presented in **Figure 5a** calculates the amount of Fe bound to secondary oxyhydroxides through subtraction of all other iron forms from the measured soil total Fe. However, these results are strictly supported by our mineralogical analyses, showing the greatest levels of goethite in the felsic woodland soils (**Figure 2b**).

Soil organic matter and its associated soil organic carbon (SOC) stocks increase along the seral stages (**Figure 5b**). In soils derived from predominantly mafic parent material, SOC

levels are lowest in bare ground soils averaging only 0.66%; in grasslands soil organic carbon (SOC) increases to 2.80% with levels culminating in woodland soils at 3.94% (**Figure 5b**). Interestingly, comparing felsic with mafic woodland soils, the felsic systems (7.73%) exhibited ~2-fold greater SOC than their mafic counterparts (**Figure 5b**). Converting these SOC concentrations to absolute stocks, we found that these SOC stocks ranged from 19 $tCO_2eq.\ ha^{-1}$ in bare ground soils to 227 $tCO_2eq.\ ha^{-1}$ in felsic woodland soils (**Figure 5b**).

In order to explore the origins of the increase in SOC in felsic systems, and in particular, to investigate if the increase could be linked to higher incidence of particulate organic carbon (POC), typically associated with greater C:N ratios [34], we measured the C:N ratios of woodland soils. We find that there was no statistically significant difference (two-tailed unpaired t-test, $P = 0.22$) in the C:N ratio of felsic (mean = 12.58) and that of mafic woodland soils (mean = 12.04; **Supplementary Figure 3**). These results indicate that POC is an unlikely source to the significant difference in SOC at the two woodland soil systems. The other central pool of SOC is made up of mineral-associated organic carbon (MAOC)[35]. MAOC represents soil organic matter that has been bound to and occluded in fine-sized, colloidal minerals [36]. Next, we calculated the sum of colloidal minerals, typically clays and iron oxyhydroxides, in our soils (**Figure 5c**). We find that the felsic system contains a greater total of colloidal minerals, both clays and goethite, than all of the mafic systems (**Figure 5c**). However, our correlational analyses (**Figure 5d-f**) show that goethite but not clays positively correlated significantly with measured SOC levels (Pearson's correlation test, $P < 0.05$). These findings held valid both at the whole-site level (**Figure 5d**) as well as when analyses were carried out only on the subset of woodland soils (**Figure 5e,f**).

Using selective chemical extractions of soils, we also investigated for the presence of manganese (Mn) oxyhydroxide minerals (e.g., birnessite) and poorly crystalline Fe oxyhydroxide minerals (e.g., ferrihydrite) that are typically of low abundance (<0.1-0.2% wt.) and thus difficult to detect by XRD and FTIR mineralogical analyses. Our analyses from the selective extractions revealed that the procedure leached substantial amounts of Fe from the primary mineral phase of fresh rocks (higher than from soils), making it difficult to distinguish between leached Fe from primary minerals and secondary Fe oxyhydroxides (**Supplementary Figure 4**). As such selective extractions appear not well suited for our soils rich in primary Fe minerals. However, our selective extractions indicated that Mn levels in felsic soils (~643 mg kg^{-1}) were greater than these leached from either of the parent fresh rocks (basalts: 416 mg kg^{-1}, dacites: 46 mg kg^{-1}). After accounting for leaching from primary phases, these results reveal that ~49% of total soil Mn (~471 mg Mn kg^{-1} or ~0.081% wt. birnessite) in these felsic soils had been converted to secondary Mn oxyhydroxides (**Supplementary Figure 4**). In contrast, in mafic woodland soils, the selectively extracted Mn levels were near their expected baseline, suggesting no or limited amount of Mn oxyhydroxide formation. Combined with our mineralogical analyses, these findings suggest that crystalline Fe oxyhydroxides (goethite) and Mn oxyhydroxides may both contribute to the 2-fold increases in SOC reported for the felsic soils at our site, with secondary Fe phases being of greater quantitative importance (3.163% wt. goethite in felsic soils).

Discussion

Saturation dynamics in the Chatala system

Our interpretation for the factors that contributed to the pattern of more advanced weathering in soils predominantly from felsic materials relative to soils predominantly from mafic materials is first and foremost saturation. The Chatala volcanic hill is in the steppe region of Bulgaria [37], characterized by warm temperate climate with long and dry summers and mean annual precipitation of around 500-600 mm [38]. These warm and dry conditions together with the large amounts of basalt stocks and the impermeability of the igneous parent material define conditions of relatively high saturation in basic cations in soil solutions. These conditions are conducive for the formation of smectitic clays [39], particularly these of trioctahedral configuration such as saponites that require high Fe and Mg activity as opposed to these of dioctahedral configuration such as montmorillonites/beidellites [40]. Consequently, saponites often dominate the clay fraction in altered rocks [40]. However, their presence in soils is rare as most volcanic regions studied either have more mature soils (where saponite may have been converted to clays poorer in cations [41]) and/or are in wetter temperate or tropical climates where weathering rates are faster [39],[40]. Nevertheless, they make up a large percentage of the clay fraction in soils derived from macrocrystalline basic rocks (amphibolites, gabbro) or ultra-basic rocks (e.g., lherzolite) where the localized saturation may be reached due to the high amount of ferromagnesic minerals as well as including their coarser size (e.g., gabbro)[40]. To illustrate that point further, in Belbex, France, soils derived from basalt weathering often contain dioctahedral smectites, halloysite and Fe-Mn oxides, while saponite is only found in the altered fractured bedrock [40]. However, mean annual precipitation at Belbex is around 1100 mm [42]– almost twice that of our system – and is thus conceivable that saponites, clays requiring greater saturation for their stable formation, may be more abundant in the drier volcanic soils at the Chatala hill.

Our rocks, particularly the mafic end-members, contain a high concentration of Ti, determined in part by the abundance of titania-rich augite (titanaugite). Ti-rich augite typically exhibits lower weathering rates compared to conventional augite [43] – a trend that helps explaining the relative stability and continued presence of augite in our soils (**Figure 2a**). Therefore, mineralogical specificities together with saturation kinetics may both be responsible for the longevity of certain primary mineral phases in our system (**Figure 4**).

Consequently, our soils, even the deeper, more developed mafic woodland soils, still contain a sizeable fraction of magnetic rock fragments/grains (~23% wt.), rich in unweathered primary minerals. In comparison, the felsic woodland soils contained over 7-fold lower amount of magnetic rock fragments/grains (~3% wt.). The composition of the extracted and crushed magnetic grains is suggestive of a weathered basaltic composition. Moreover, these findings show that although the two systems started at ~2.5-fold difference in magnetic basalts (~81% in mafic systems, ~33% in felsic systems), the more favourable weathering kinetics in the felsic system brought this up to a 7-fold difference in magnetic basaltic elements. This finding of faster basaltic loss in the felsic systems is in further support of greater loss in major cations in felsic systems (**Figure 4**), more pronounced goethite accumulation in felsic system (**Figure 5**),

all indicative of faster weathering kinetics of basaltic stocks in the felsic system than in the mafic system and more advanced weathering stages.

Base saturation on exchange sites is still quite high in our system with all of our soils revealing levels >97% (**Figure 3a**). These results show that natural systems, devoid of the acidifying potential of ammoniacal N-fertilizers (strong acid)[44], build up exchangeable acidity rather slowly. It is conceivable that the saturation in primary minerals and the lack of strong acid weathering both contribute to relatively unfavourable weathering kinetics while contributing to favourable kinetics for the formation of clay-rich phases. To expand on this, our soils are of a high clay component (30-40% wt.) and in turn a high exchangeable pool of cations (>40-60 $cmol^{+}\ kg^{-1}$). Together, these likely result in equally high cation concentrations in soil solutions, with these saturated solutions demoting the further weathering of primary minerals.

The combination of low precipitation, warm and dry summer period, cation-rich volcanic rock parent material and mineralogy (e.g., titanaugite vs. augite) all have acted as bottleneck factors limiting the export of alkalinity and $CDR_{alkalinity}$ from the Chatala volcanic system. At the same time, these have favoured the formation of extensive smectitic clay component of high cation content (both exchangeable and structural), that created volcanic soils of relatively high fertility and pool of exchangeable nutrients (**Figure 3a, Figure4d**).

Soil organic carbon accumulation in the Chatala system

Our findings point to a step-wise increase in SOC in the Chatala volcanic hill – moving from the least developed bare ground soil to our more developed woodland soils in line with a more pronounced presence of complex plant life (**Figure 5b**).

The weathering of volcanic rocks is known to contribute to the formation of mineral-associated organic matter (MAOM). The MAOM formation is mechanistically understood to proceed through the charge-based (polar) and apolar interactions of soil organic molecules with colloidal minerals – mainly clays and Fe oxyhydroxides [45],[46]. Positively charged organic molecules (e.g., amino acids, proteins, nucleotides), in accordance with their dissociation constants, exhibit positive charge at acidic pH (pH < 6 for nucleotides and some amino acids such as histidine, pH < 3 for other amino acids such as glycine, glutamate). Therefore, polar binding between the typically negatively charged clays and these organic molecules is mainly limited to the acidic pH range. Although apolar binding can occur, it is of relatively limited extent, ranging to 5-10% adsorption of added organics [47].

The charge of colloidal Fe oxyhydroxide minerals such as goethite is pH-variable. Typically, they are positively charged at pH < 7, with negative charges increasing as pH reaches neutral and beyond [48]. Consequently, at the pH of our soils (pH 6.4-6.8), newly formed goethite will contain mainly positive charges and thus bind predominantly negatively charged soil organic molecules. A large fraction of soil organic molecules is negatively charged at the pH of soils owing their content of carboxylic groups ($R\text{-}COOH \leftrightarrow H^{+} + R\text{-}COO^{-}$), these include humic substances (e.g., humic acids, fulvic acids), tannic acid, benzoic acid, oxalic acid, citric acid, etc. [46]. Smectitic clays can also exhibit amphoteric pH-variable charges at their OH

edges but their extent represents only 10-30% of the net clay charge and positive charges are only limited to pH < 6.5 [49].

The listed adsorption specificities of goethite and smectitic clays and the slightly acidic-nearly neutral pH of our soils together likely underline the observation that the extended formation of MAOM in our system was mainly attributable to and correlating with goethite, with a more limited contribution of the clays revealed by a lack of significant correlation (**Figure 5d-f**).

The formation of goethite is of greatest extent in the felsic soils (**Figure 5a,c**). In turn, the higher goethite content of felsic soils governs the stabilisation of soil organic matter and its SOC stocks in the felsic soils (**Figure 5b**) through the formation of recalcitrant MAOM. It is noteworthy that the more extensive formation of goethite in soils derived from parent materials of high felsic/mafic ratio (felsic soils) relative to soils of low felsic/mafic ratios (mafic soils) may be counterintuitive at first given that mafic rocks are richer in ferromagnesian minerals than felsic rocks (**Figure 2b**) and thus contain higher total Fe than their felsic counterparts (**Figure 1d**). This apparent conundrum is resolved when the two systems are analysed through the prism of saturation and weathering kinetics. The faster weathering kinetics of the basaltic materials in the felsic soils compared to the basaltic materials in the mafic soils result in the felsic soils reaching advanced weathering stages more rapidly. Consequently, goethite, a product typical of more advanced weathering stages **(Figure 5a)** [32],[33], peaks in the felsic soils despite their lower total Fe. Another mechanism promoting the formation of goethite in the felsic system may be the higher formation of illite/smectite mixed layer clays which are of typically lower Fe content than saponites thus incorporating less Fe in clay lattices (**Figure 4d**). The preferential formation of illite/smectite relative to saponite in the felsic system may be in turn be caused by inherent differences in mineralogy (more feldspars), chemical composition (higher K), and saturation (lower) in the felsic soils. The medium-to-long-term stability of any such formed SOC-goethite complexes as part of the MAOC/M in the felsic soils is strengthened by the relatively limited Fe(III)-reduction cycling. The limitation to the Fe cycle is in turn likely caused by the relative dry climate and geologically young soil setting.

Concluding remarks – recommendations for ERW trials

1. Estimating CDR

Current ERW trials often estimate potential CDR (CDR_{pot}) through the loss of cations from applied rock feedstocks. This may be misleading because, as we demonstrate here, the sizeable incorporation of major cations in secondary clay phases and absorption onto soil exchangers can amount to 23-48% of all major cations in the system at baseline levels and at the same time represent 60-70% of all cations lost from rock feedstocks. Further, we demonstrate that upon saturation, these pools may represent medium to long-term cation sinks – stable over decadal to even millenial timescales. Therefore, we recommend that ongoing and future ERW trials apply more rigorous soil pore water/tile drain sampling for constraining their alkalinity-driven CDR ($CDR_{alkalinity}$). Alternatively, deeper soil sampling (>30-120+ cm) may be recommended to account for the increases in exchangeable and clay pools deeper in the soil profile that can then be deducted from CDR_{pot} to arrive at a more realistic approximation of $CDR_{alkalinity}$.

2. Saturation kinetics ("less is more")

Our findings show that greater alkalinity fluxes are generated over time in systems of higher felsic/mafic ratios (140 $tCO_2eq.\ ha^{-1}$) than in systems of lower felsic/mafic ratios, dominated by mafic parent inputs (up to 101 $tCO_2eq.\ ha^{-1}$). Furthermore, SOC accumulation and the formation of MAOM more readily occurs in felsic soils owing their extended precipitation of goethite. As many of the soils host to ERW trials are of felsic-like composition (high in resistant mineral phases such as quartz and K-feldspars), maintaining a favourably low felsic/mafic ratio can easily be achieved by avoiding over-application of mafic basaltic feedstocks (e.g., applying 5 $t\ ha^{-1}\ yr^{-1}$ for 25 years, than applying 25 $t\ ha^{-1}\ yr^{-1}$ for 5 years). Alternatively, feedstocks of naturally low felsic/mafic ratios may be preferred for ERW applications (e.g., basaltic andesite or andesites than basalts). Lastly, mixing the applied rock feedstocks well with the host soils through tilling may be preferred compared to surface application. Doing this would avoid the formation of a surface layer of almost pure mafic composition, one closely resembling the pedogenesis of our mafic soils with their associated saturation.

2. Saturation kinetics ("less is more")

Our findings show that greater alkalinity fluxes are generated over time in systems of higher felsic/mafic ratios (140 $tCO_2eq.\ ha^{-1}$) than in systems of lower felsic/mafic ratios, dominated by mafic parent inputs (up to 101 $tCO_2eq.\ ha^{-1}$). Furthermore, SOC accumulation and the formation of MAOM more readily occurs in felsic soils owing their extended precipitation of goethite. As many of the soils host to ERW trials are of felsic-like composition (high in resistant mineral phases such as quartz and K-feldspars), maintaining a favourably low felsic/mafic ratio can easily be achieved by avoiding over-application of mafic basaltic feedstocks (e.g., applying 5 $t\ ha^{-1}\ yr^{-1}$ for 25 years, than applying 25 $t\ ha^{-1}\ yr^{-1}$ for 5 years). Alternatively, feedstocks of naturally low felsic/mafic ratios may be preferred for ERW applications (e.g., basaltic andesite or andesites than basalts). Lastly, mixing the applied rock feedstocks well with the host soils through tilling may be preferred compared to surface application. Doing this would avoid the formation of a surface layer of almost pure mafic composition, one closely resembling the pedogenesis of our mafic soils with their associated saturation.

Methods and materials

Study site information

The Chatala volcanic hill site is located in the central part of Northern Bulgaria, decimal geographic coordinates: 43.280075, 25.210872. The climate in this part of Bulgaria is characterized as warm temperate with low mean annual precipitation of 500-600 mm and mean annual temperature of 12.33ºC [38]. Phytogeographically, this part of Bulgaria represents the forest-steppe mix of dry grasslands and woodland patches [37]. At the site, the soils are of brown-gray colouration [22] and can be classified as Entisols due to their characteristic absence of genetically distinct horizons [50]. The volcanic hill is one of a series of volcanic hills/mounds, a total of between 17 to 23, in Northern Bulgaria, believed to be related to a single volcanic event during the Neogene [21],[51].

Rock and soil collection

Rocks (total $n = 9$ rock samples) were collected from several exposed rock facies on the top of the Chatala hill including some that have been found as large hand specimens in the volcanic scree formed immediately underneath the peak which was also sampled (gravel, $n = 3$ samples). Soils were sampled from 0-10 cm depth using a shovel and ruler and placed in labelled ziplock bags. Soils were acquired from three distinct plant communities, in a close proximity of a few hundred meters of each other – bare ground (of no to little vegetation – mainly lichens, mosses, and the occasional grass, $n = 3$ soil samples), grassland (short grasses, $n = 3$ soil samples), and woodland (composed of Hungarian oak, *Quercus frainetto* and Oriental hornbeam, *Carpinus orientalis*, $n = 3$ soil samples for each tree species to a total of $n = 6$ woodland soil samples). The woodland samples were collected, 20 cm away from the main tree trunk, from the under-crown area of the tree. Our subsequent analyses revealed that 1 of the 3 oak soil samples belonged to the dacitic soils, with the other 2 belonging to the mafic soils. In the collected hornbeam soil samples, 2 were classified as dacitic and 1 as mafic. Consequently, throughout the manuscript we did not distinguish between tree species but rather based our grouping of the woodland soils according to their parent material composition ($n = 3$ for mafic woodland soils and $n = 3$ for felsic woodland soils).

Soil processing and magnetic separation

Soils were air-dried and sieved < 2 mm. Aliquots of the sieved soils were then subjected to magnetic separation using strong neodymium magnets [10]. The magnetic separation, designed to pull basalt out from ERW trial soils, works by selectively extracting the magnetite-rich partially weathered basalt grains from the rest of the soil matrix after a series of sequential extractions. These figures were useful for estimating the partially weathered component of primary minerals of basaltic origin and comparing it against the estimates derived through detailed cation budgets. Unseparated bulk soils and magnetic basaltic grains were homogenized using agate pestle and mortar. The latter were cleaned with 100% ethanol in between samples. Rock samples were pre-crushed using a hammer-ball crusher to smaller fragments. Fragments were selected from the core of the cracked rock samples as to avoid the exterior altered weathering rind and thus analyse only the fresh unaltered composition of the interior. These fragments were then crushed using an agate ball mill at maximum speed for 3-5 minutes. Each crushed rock was screen to pass through a 63 µm sieve. The crushed samples were further dried in the oven at 50^{o}C for a few days and then stored in a desiccator.

Spectroscopic analyses of rocks and soils – XRF, FTIR, XRD

The crushed, homogenized and dried rock and soil samples were then subjected to X-ray fluorescence (XRF) and Fourier Transform Infrared (FTIR) spectroscopy. For XRF, crushed material was decanted into a specifically designed mini-sample holder. The latter is made of a plastic 15 ml tube (internal diameter = 1.7 cm) that is cut at 7 from the neck. The bottom of the cut sample holder was then covered with an XRD-grade Mylar® polyethylene film tightened with the help of an O-ring. The resulting mini-sample holder is more suitable for small sample volumes as its small diameter covers the window of the XRF analyzer (~1.5 cm) without leaving much unanalysed surface area. The XRF analyses were performed using a portable XRF (Thermo Scientific Niton XL2t GOLDD+) mounted on a safety stand and operated remotely. Each sample was analysed three times (after each run the sample was mixed to scan a new sample "face") and its average elemental composition derived from the three runs. The scanning was performed in Cu/Zn mining mode and included a 30 s heavy element scan and a 60 s light element scan. The XRF results were calibrated against the BHVO2 basalt standard and its published literature values.

The FTIR spectra were obtained in Attenuated Total Reflection (ATR) mode on a Thermo Scientific Nicolet iS50 spectrometer fitted with a Smart ITR Diamond monolith accessory. The sample was placed back in its tube at the end of each its spectrum collection and the diamond probe pedestal was wiped cleaned in between runs with 100% ethanol. Each sample spectrum was the average of 60 FTIR scans taken at 4 cm^{-1} resolution. The scans were collected using the Thermo Scientific Omnic software and then analysed in SpectraGryph 1.2. The spectra were baseline corrected using linear normalisation and offset to 0.

X-ray diffraction (XRD) spectroscopy of a subset of samples ($n = 6$, one bare ground soil, one grassland soil, one mafic woodland soil, one felsic woodland soil, a basaltic rock sample and a dacitic rock sample) was carried out at the X-ray Diffraction Lab at the James Hutton Institute, University of Aberdeen, UK. For bulk (whole sample) quantitative analysis samples are wet ground for 12 minutes (in ethanol or water) in a McCrone mill and oven dried following milling. X-ray powder diffraction (XRPD) patterns are typically recorded over a range of 65°2θ or more using Cu radiation, the actual range being instrument dependent is given on the scans. Quantitative analysis is made by a normalised full pattern reference intensity ratio (RIR) method as described in [52],[53]. Unless stated otherwise, expanded uncertainty using a coverage factor of 2, i.e. 95% confidence, is given by ±X^0.35, where X = concentration in wt.%., e.g. 30 wt.% ±3.3.

Partial least square (PLS) model for mineralogy predictions based on ATR-FTIR spectra and its validation against XRD data

The generated XRD mineralogy was used to first identify the main minerals across the samples. These included the following primary mineral phases: olivine, pyroxene, plagioclase, K-feldspar, quartz, thomsonite, phillipsite, analcime, apatite, anatase, trioctahedral mica, trioctahedral chlorite, and magnetite. In addition, the following secondary phases were identified: goethite,

trioctahedral smectites, and illite/smectite mixed layer clays. Based on the list of identified minerals, 20,000 random theoretical mixture spectra were derived using a combination of individual mineral spectra collected in our lab using mineral standards (olivine, pyroxene /augite/, quartz, chlorite /ripidolite/, magnetite, trioctahedral mica /biotite/, illite/smectite mixed layer clays, trioctahedral smectites /saponite/, goethite, volcanic glass) or spectra from the RRUFF mineral database [54] (the remaining minerals). The resulting 20,000 theoretical mineral mixture spectra were passed for training of a PLS model [55] adjusted to exclude negative values. Several PLS models were developed through exclusion/inclusion of certain identified minerals during the creation of the theoretical mixture spectra. The best model was selected through its ability to reliably predict the mineral composition in the subset of samples analysed through XRD. The final model contained the following minerals: augite, magnetite, quartz, fluorapatite, K-feldspar (sanidine), volcanic glass, illite-smectite (70-30), saponite, goethite, thomsonite, calcite, nepheline, olivine, plagioclase (anorthite and albite). The reliability of predictions was assessed using Pearson's correlation tests with the resulting Pearson's *r* values reported in Figure 2A. Clay source minerals were acquired from The Clay Minerals Society. The remaining minerals were acquired from various mineral vendors. For validation against its purported label, each purchased mineral was ATR-FTIR-scanned and searched against the RRUFF database and only mineral positively matching minerals were further used.

Exchangeable and selective extractions

The effective cation exchange capacity (eCEC) was determined through extractions with dilute solutions of cobalt (III) hexamine trichloride (Cohex) as outlined in previous work [56],[57] with slight modifications. Briefly, 0.5 g of ground soil/rock was mixed with 10 mL of 0.0166 M Cohex solution and mixed on an end-over-end shaker at 40 rpm for 1 hour. Extracted samples were centrifuged at 4,700 x *g* for 2 minutes and the supernatant solutions were syringe-filtered through 0.45 µm filters. Subsequently, eCEC values were determined both using (a) spectrophotometric approach (scanning sample solutions at wavelength of 475 nm and comparing it against blank solutions of Cohex) and (b) through Co adsorption to the exchange site (determined as the difference between the Co concentration in blank Cohex solutions and that of the reacted samples). The concentration of Co and major cations were measured in the filtered exchanged solutions using through inductively coupled plasma mass spectroscopy (ICP-MS)[10] at the School of Biosciences, University of Nottingham, UK.

The amounts of amorphous and poorly crystalline Fe and Mn oxyhydroxides were determined through selective extractions of soils/rocks with 0.25 M hydroxylamine hydrochloride dissolved in 0.25 M hydrochloric acid using previously published methodology [35],[58],[59]. The elemental concentration of solutions was analysed through ICP-MS.

Soil total carbon and nitrogen analyses

Untreated soil samples and acid-stripped soil samples (carbonates removed by reaction with 6 M HCl for 24 h in a fume cabinet, followed by 48 h of drying at 50^{o}C in an extraction oven) were weighted to aliquots of 20-40 mg and placed in aluminium foil packets carefully closed with tweezers. The resulting packets were checked for leaks and were then loaded onto a Elementar CN analyser calibrated with acetanilide (C:N = 8) for high-temperature Dumas combustion method for measuring C and N content.

Calculating CDR pools

Each of the subsidiary CDR pools (realized, exchangeable, clays, primary minerals) were calculated using the same approach. The loss of cations for $CDR_{realized}$ was calculated as the difference between the baseline cation stocks (derived from basalt and dacite mixing) and current cation stocks in soils (as measured by our total elemental analyses). The CDR held on exchangeable sites was calculated from the concentration of exchangeable cations as indicated by our exchangeable extractions. The CDR held in clays was obtained through XRF analysis of saponite collected through careful scraping from the rock gravel samples at our site (Figure 1), while illite-smectite approximate composition was derived from subtraction of other mineral phases from the total soil composition using idealized mineral chemical composition [60]. The CDR held in primary minerals was calculated as the product of the subtraction of all so-far-listed CDR pools from the CDR_{total}.

References

1. Polynov BB. 1937 *The Cycle of Weathering*. Moscow: T. Murby.
2. Weil RR, Brady NC. 2017 *The Nature and Properties of Soils*. 15th ed. Pearson.
3. Uroz S, Calvaruso C, Turpault MP, Frey-Klett P. 2009 Mineral weathering by bacteria: ecology, actors and mechanisms. *Trends Microbiol.* **17**, 378–387. (doi:10.1016/j.tim.2009.05.004)
4. Smits MM, Johansson L, Wallander H. 2014 Soil fungi appear to have a retarding rather than a stimulating role on soil apatite weathering. *Plant Soil* **385**, 217–228. (doi:10.1007/s11104-014-2222-6)

5. Tice KR, Graham RC, Wood HB. 1996 Transformations of 2:1 phyllosilicates in 41-year-old soils under oak and pine. *Geoderma* **70**, 49–62.
6. Macedo MO, Resende a. S, Garcia PC, Boddey RM, Jantalia CP, Urquiaga S, Campello EFC, Franco a. a. 2008 Changes in soil C and N stocks and nutrient dynamics 13 years after recovery of degraded land using leguminous nitrogen-fixing trees. *For. Ecol. Manage.* **255**, 1516–1524. (doi:10.1016/j.foreco.2007.11.007)
7. Adisaputro D, De Donato P, Saint-Andre L, Barres O, Galy C, Nourrisson G, Piedevache M, Derrien M. 2021 Baseline subsoil CO2 gas measurements and micrometeorological monitoring: Above canopy turbulence effects on the subsoil CO2 dynamics in temperate deciduous forest. *Appl. Sci.* **11**, 1–19. (doi:10.3390/app11041753)
8. Epihov DZ *et al.* 2024 Iron Chelation in Soil: Scalable Biotechnology for Accelerating Carbon Dioxide Removal by Enhanced Rock Weathering. *Environ. Sci. Technol.* **58**, 11970–11987. (doi:10.1021/acs.est.3c10146)
9. White AF, Brantley SL. 2003 The effect of time on the weathering of silicate minerals: Why do weathering rates differ in the laboratory and field? *Chem. Geol.* **202**, 479–506. (doi:10.1016/j.chemgeo.2003.03.001)
10. Beerling DJ *et al.* 2024 Enhanced weathering in the US Corn Belt delivers carbon removal with agronomic benefits. *Proc. Natl. Acad. Sci.* **121**, e2319436121. (doi:10.1073/pnas)
11. Beerling DJ *et al.* 2025 Transforming US agriculture for carbon removal with enhanced weathering. *Nature* (doi:10.1038/s41586-024-08429-2)
12. Li C, Kang S, Gao Y. 2025 Rethinking CO2 Removal Efficiency in Enhanced Rock Weathering. *Environ. Sci. Technol.* **59**, 8878–8880. (doi:10.1021/acs.est.5c03802)
13. Larkin CS *et al.* 2022 Quantification of CO2 removal in a large-scale enhanced weathering field trial on an oil palm plantation in Sabah, Malaysia. *Front. Clim.* **4**. (doi:10.3389/fclim.2022.959229)
14. 2022 The 'Cartion Park' Model for ERW on Croplands. *Carbon Draw. Initiat.* , 1–14. See https://www.carbon-drawdown.de/blog/2022-12-7-the-cartion-park-model-for-erw-on-croplands (accessed on 10 December 2024).
15. Xu T *et al.* 2025 Enhanced Rock Weathering Promotes Soil Organic Carbon Accumulation: A Global Meta-Analysis Based on Experimental Evidence. *Glob. Chang. Biol.* **31**. (doi:10.1111/gcb.70483)
16. Wang Q, Zhu C, Yun J, Yang G. 2017 Isomorphic Substitutions in Clay Materials and Adsorption of Metal Ions onto External Surfaces: A DFT Investigation. *J. Phys. Chem. C* **121**, 26722–26732. (doi:10.1021/acs.jpcc.7b03488)
17. Epihov DZ, Saltonstall K, Batterman SA, Hedin LO, Hall JS, van Breugel M, Leake JR, Beerling DJ. 2021 Legume-microbiome interactions unlock mineral nutrients in regrowing tropical forests. *Proc. Natl. Acad. Sci. U. S. A.* **118**, 1–29. (doi:10.1073/pnas.2022241118)
18. Batterman S a, Hedin LO, van Breugel M, Ransijn J, Craven DJ, Hall JS. 2013 Key role of symbiotic dinitrogen fixation in tropical forest secondary succession. *Nature* **502**, 224–7. (doi:10.1038/nature12525)
19. Zhang GL, Pan JH, Huang CM, Gong ZT. 2007 Geochemical features of a soil chronosequence developed on basalt in Hainan Island, China. *Rev. Mex. Ciencias Geol.* **24**, 261–269.
20. He Y, Li DC, Velde B, Yang YF, Huang CM, Gong ZT, Zhang GL. 2008 Clay minerals in a soil chronosequence derived from basalt on Hainan Island , China and its implication for pedogenesis. *Geoderma* **148**, 206–212. (doi:10.1016/j.geoderma.2008.10.007)
21. Marchev P, Saltikovski A, Yanev Y, Daieva L, Genshaft J. 1992 Petrology of the Neogene alkali basalts and included ultramafic xenoliths of the Moesian Platform, North Bulgaria. *Neues Jahrb. Miner. Abh.* **164**, 113–137.
22. Petrov G. 2014 Landscape-Geophysical Characteristics of the Basalt Hills in Northern Bulgaria. *Probl. Geogr.* **3**–**4**, 60–75.
23. Heimsath AM, Dietrich WE, Nishiizumi K, Finkel RC. 1997 The soil production functon and landscape equilibrium. *Nature* **388**, 49.
24. 1960 *Soils of Bulgaria*. Sofia: Zemizdat.
25. Gilkes RI, Mckenzie RM. 1988 Geochemistry and Mineralogy of Manganese in Soils. In *Manganese in Soils and Plants*, pp. 23–35. Kluwer Academic Publishers.
26. Goldich SS. 1938 A Study in Rock-weathering. *J. Geol.* **46**, 17–58.
27. Ismadji S, Soetaredjo FE, Ayucitra A. 2015 *Clay Materials for Environmental Remediation*. Springer. (doi:10.1007/978-3-319-16712-1_1)
28. Tiab D, Donaldson E. 2024 *Petrophysics: theory and practice of measuring reservoir rock and fluid transport properties*. Elsevier.
29. Manuella FC, Carbone S, Barreca G. 2012 Origin of saponite-rich clays in a fossil serpentinite-hosted hydrothermal system in the crustal basement of the Hyblean Plateau (Sicily, Italy). *Clays Clay Miner.* **60**, 18–31. (doi:10.1346/CCMN.2012.0600102)
30. Baldermann A, Dohrmann R, Kaufhold S, Nickel C, Letofsky-Papst I, Dietzel M. 2014 The Fe-Mg-saponite solid solution series – a hydrothermal synthesis study. *Clay Miner.* **49**, 391–415. (doi:10.1180/claymin.2014.049.3.04)
31. Simonsson M, Hillier S, Öborn I. 2009 Changes in clay minerals and potassium fixation capacity as a result of release and fixation of potassium in long-term field experiments. *Geoderma* **151**, 109–120. (doi:10.1016/j.geoderma.2009.03.018)
32. Blume HP, Schwertmann U. 1969 Genetic Evaluation of Profile Distribution of Aluminium, Iron, and Manganese Oxides. *Soil Sci. Soc. Am. J.* **33**, 438–444.
33. Hadjiyanakiev A. 1989 *Iron in Bulgarian Soils*. Sofia: Zemizdat.
34. Janzen HH, Campbell CA, Brandt SA, Lafond GP, Townley-Smith L. 1992 Soil microbiology & biochemistry: light-fraction organic matter in soils from long-term crop rotations. *Soil Sci. Soc. Am. J.* **56**, 1799–1806.
35. Wagai R, Mayer LM, Kitayama K, Shirato Y. 2013 Association of organic matter with iron and aluminum across a range of soils determined via selective dissolution techniques coupled with dissolved nitrogen analysis. *Biogeochemistry* **112**, 95–109. (doi:10.1007/s10533-011-9652-5)
36. Chen C, Hall SJ, Coward E, Thompson A. 2020 Iron-mediated organic matter decomposition in humid soils can counteract protection. *Nat. Commun.* **11**, 1–13. (doi:10.1038/s41467-020-16071-5)
37. Dodev Y, Georgiev G, Georgieva M, Ivanov V, Georgieva L. 2025 A Methodological Approach for the Integrated Assessment of the Condition of Field Protective Forest Belts in Southern Dobrudzha, Bulgaria. *Forests* **16**, 1–18. (doi:10.3390/f16071184)
38. Marinova T, Malcheva K, Bocheva L, Trifonova L. 2017 Climate profile of Bulgaria in the period 1988-2016 and brief climatic assessment of 2017. *Bulg. J. Meteorol. Hydrol.* **22**, 2–15.
39. Eberl DD. 1984 Clay mineral formation and transformation in rocks and soils. *Philos Trans R Soc L. A* **311**, 241–257.
40. Righi D, Meunier A. 1995 Origin of Clays by Rock Weathering and Soil Formation. In *Origin and Mineralogy of Clays*, pp. 43–161. Springer-Verlag Berlin Heidelberg.
41. Peternella WS, Costa ACS da. 2021 Evaluation of a Toposequence of Soils Derived from Basalt by Fourier Transform Infrared Spectroscopy. *OALib* **08**, 1–17. (doi:10.4236/oalib.1107867)
42. Prudhomme C, Wallingford C, Sauquet E, Lyon C. 2007 Modelling a regional drought index in France.

43. Eggleton RA, Foudoulis C, Varkevisser D. 1987 Weathering of Basalt: Changes in Rock Chemistry and Mineralogy. *Clays Clay Miner.* **35**, 161–169. (doi:10.1346/CCMN.1987.0350301)
44. Dai Z *et al.* 2018 Long-term nitrogen fertilization decreases bacterial diversity and favors the growth of Actinobacteria and Proteobacteria in agro-ecosystems across the globe. *Glob. Chang. Biol.* **24**, 3452–3461. (doi:10.1111/gcb.14163)
45. Gerasimov IP, Glazovskaya MA. 1965 *Fundamentals of Soil Science and Soil Geography*. Moscow: Gosudarstvennoe Izdatelstvo Geographicheskoi Literatury.
46. Oades JM. 1989 An Introduction to Organic Matter in Mineral Soils. In *Minerals in Soil Environments*, pp. 89–159. Soil Science Society of America.
47. Ramírez-Vazquez L, Duarte-Ruiz AA, Santiago-Santos MG, Cordero Tercero G, Cruz-Castaneda JA. 2025 Stability of adenine in interaction with saponite in a simulated hydrothermal impact-generated system and its implications for astrobiology. *Planet. Space Sci.* **264**. (doi:10.1016/j.pss.2025.106151)
48. Cornell RM, Schwertmann U. 2003 *The Iron Oxides*. Weinheim: Wiley-VCH Verlag. (doi:10.1016/j.anucene.2015.08.018)
49. Mermut AR, Lagaly G. 2001 Baseline studies of the clay minerals society source clays: Layer-charge determination and characteristics of those minerals containing 2:1 layers. *Clays Clay Miner.* **49**, 393–397. (doi:10.1346/CCMN.2001.0490506)
50. USDA. 1999 *Soil Taxonomy - A Basic System of Soil Classification for Making and Interpreting Soil Surveys*. Second edi. (doi:10.1007/BF01574372)
51. Velchev A. 1972 Morphology of basalt mounds in Northern Bulgaria. *Proc. Bulg. Geogr. Community* **12**, 29–44.
52. Omotoso O, McCarty DK, Hillier S, Kleeberg R. 2006 Some successful approaches to quantitative mineral analysis as revealed by the 3rd reynolds cup contest. *Clays Clay Miner.* **54**, 748–760. (doi:10.1346/CCMN.2006.0540609)
53. M. Butler B, Hillier S. 2021 Automated Full-Pattern Summation of X-Ray Powder Diffraction Data for High-Throughput Quantification of Clay-Bearing Mixtures. *Clays Clay Miner.* **69**, 38–51. (doi:10.1007/s42860-020-00105-6)
54. Lafuente B, Downs RT, Yang H, Stone N. 2016 The power of databases: The RRUFF project. *Highlights Mineral. Crystallogr.* , 1–29. (doi:10.1515/9783110417104-003)
55. Seybold CA *et al.* 2019 Application of Mid-Infrared Spectroscopy in Soil Survey. *Soil Sci. Soc. Am. J.* **83**, 1746–1759. (doi:10.2136/sssaj2019.06.0205)
56. Ciesielski H, Sterckeman T. 1997 Determination of cation exchange capacity and exchangeable cations in soils by means of cobalt hexamine trichloride. Effects of experimental conditions. *Agron. Agric. Environ.* **17**, 1–7. (doi:10.1051/agro:19970101)
57. Ciesielski H, Sterckeman T. 1997 A comparison between three methods for the determination of cation exchange capacity and exchangeable cations in soils. *Agronomie* **17**, 9–16. (doi:10.1051/agro:19970102)
58. Wagai R, Mayer LM. 2007 Sorptive stabilization of organic matter in soils by hydrous iron oxides. *Geochim. Cosmochim. Acta* **71**, 25–35. (doi:10.1016/j.gca.2006.08.047)
59. Ulery AL, Drees LR. 2008 *Methods of Soil Analysis: Part 1—Physical and Mineralogical Methods*. See https://dl.sciencesocieties.org/publications/books/abstracts/sssabookseries/methodsofsoilan1/901/preview.
60. 2026 Mindat - Mines, Minerals, and More. See https://www.mindat.org/ (accessed on 20 June 2002).

Main Figures

a

b

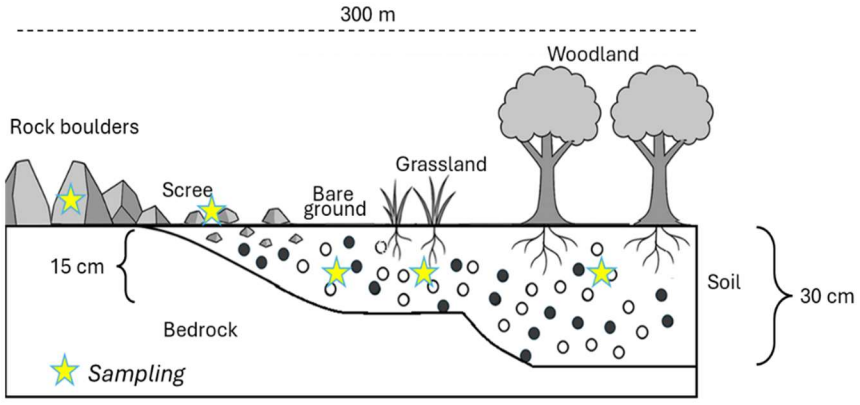

c

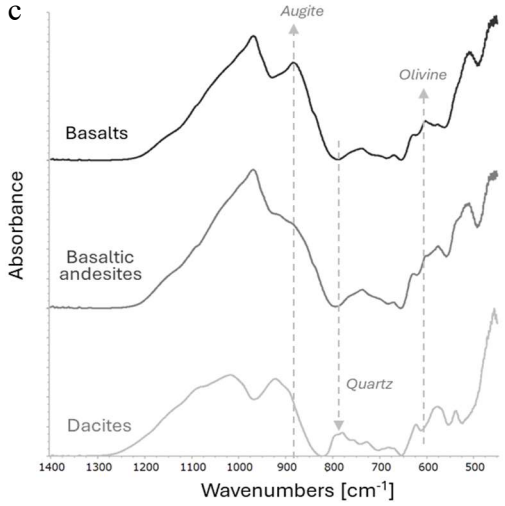

d

Oxide/ element	Basalts	Basaltic andesites	Dacites
SiO_2 %	51.57 (0.23)	54.69 (0.78)	72.92 (1.00)
Al_2O_3 %	9.88 (0.18)	10.58 (0.45)	11.38 (0.13)
Fe (mg kg^{-1})	89,344 (1,435)	79,952 (3,945)	47,638 (356)
Mg (mg kg^{-1})	56,257 (2,687)	41,065 (626)	12,251 (1,055)
Ca (mg kg^{-1})	83,272 (1,612)	81,929 (1,835)	46,414 (354)
K (mg kg^{-1})	11,413 (740)	12,063 (3,308)	27,760 (42)
Ti (mg kg^{-1})	15,518 (517)	15,181 (70)	5,865 (103)
P (mg kg^{-1})	6,944 (352)	8,572 (1,805)	1,219 (239)
Mn (mg kg^{-1})	1,359 (27)	1,226 (63)	772 (24)
Ni (mg kg^{-1})	223 (15)	138 (18)	BDL (NA)
Cr (mg kg^{-1})	353 (26)	311 (1)	BDL (NA)
Cu (mg kg^{-1})	44 (2)	39 (5)	35 (2)

Figure 1. Site layout and parent material lithology. a. Photographs of site and inlet images showing the three systems – bare ground, grassland, and woodland; **b.** Site schematic layout showing soil profile depth and sampling; **c.** Fourier Transform Infrared (FTIR) spectra of parent materials and associated major mineral peaks; **d.** Total elemental composition of parent materials.

a

Mineral-specific performance of the FTIR PLS model benchmarked against XRD analyses

	Olivine	Pyroxene	Plagioclase	Volc. glass	K-feldspar	Quartz	Saponite	Illite-Smect.	Goethite
Pearson's *r* correlation	0.923	0.938	0.979	0.882	0.423	0.944	0.912	0.811	0.906

b

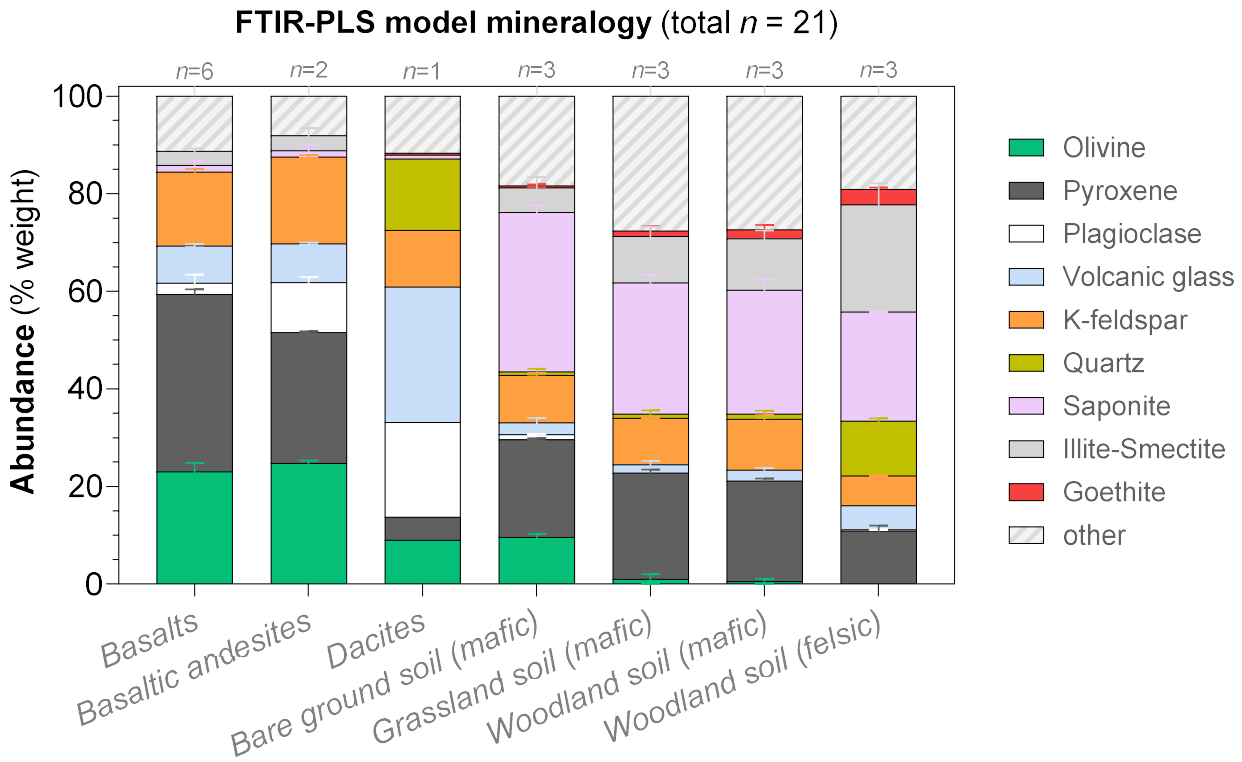

Figure 2. FTIR-based quantitative mineralogy of parent materials and soils. a. Correlation between FTIR-based mineral quantification and X-ray diffraction (XRD) data (Pearson's correlation test, shown are Pearson's *r* values); **b.** Quantitative mineralogy based on FTIR and Partial Least Square (PLS) regression model.

a

	Mafic soils			Felsic soils
	Bare ground soil (mafic)	Grassland soil (mafic)	Woodland soil (mafic)	Woodland soil (felsic)
Soil pH	6.71 (0.09)	6.67 (0.20)	6.39 (0.28)	6.83 (0.07)
Soil eCEC ($cmol^+ kg^{-1}$)	40.13 (4.31)	51.10 (4.21)	59.46 (0.94)	53.47 (3.51)
Base saturation (%)	99.82 (0.18)	98.64 (0.02)	97.93 (0.67)	97.72 (1.18)
SiO_2 %	57.02 (0.42)	57.11 (0.87)	58.74 (0.74)	67.67 (0.95)
Al_2O_3 %	10.29 (0.27)	10.33 (0.35)	10.25 (0.17)	11.69 (0.24)
Fe ($mg kg^{-1}$)	82,771 (1,597)	81,474 (1,853)	77,232 (1,356)	57,833 (1,502)
Mg ($mg kg^{-1}$)	52,003 (2336)	50,116 (2,300)	47,512 (3,236)	22,552 (1,803)
Ca ($mg kg^{-1}$)	61,163 (1,399)	62,263 (956)	57,689 (1,143)	36,256 (1,893)
Ti ($mg kg^{-1}$)	11,908 (213)	12,323 (481)	11,607 (433)	7,805 (260)
K ($mg kg^{-1}$)	15,869 (616)	15,983 (778)	21,913 (948)	29,995 (609)
P ($mg kg^{-1}$)	6,672 (223)	6,861 (636)	6,407 (437)	6,994 (414)
Mn ($mg kg^{-1}$)	1,452 (59)	1,335 (50)	1,358 (45)	1,290 (48)
Ni ($mg kg^{-1}$)	220 (11)	180 (17)	148 (12)	98 (7)
Cr ($mg kg^{-1}$)	294 (18)	323 (13)	BDL (NA)	BDL (NA)
Cu ($mg kg^{-1}$)	57 (5)	62 (8)	66 (4)	77 (7)

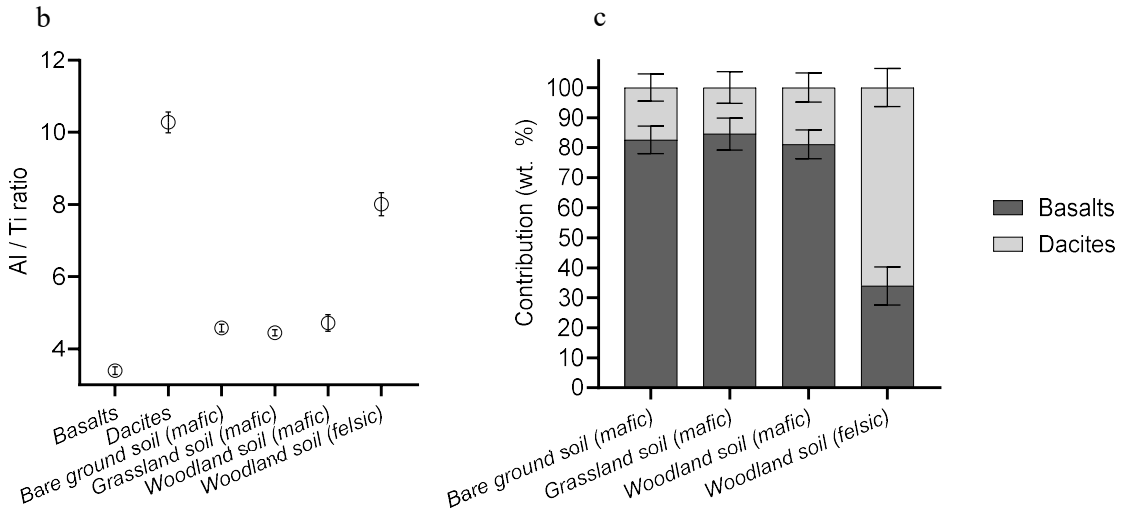

Figure 3. Total elemental composition of soils at the Chatala site and contribution of each parent material to the soils. a. Total elemental composition of soils; **b.** Al/Ti ratio shows distinct differences in the two parent materials (basalts and dacites) that are reflected in their derived soils which show values in-between the two parent material end-members – this can be used to estimate the contribution of the two end-members; **c.** Contribution of parent material end-members to each of the observed soil groups.

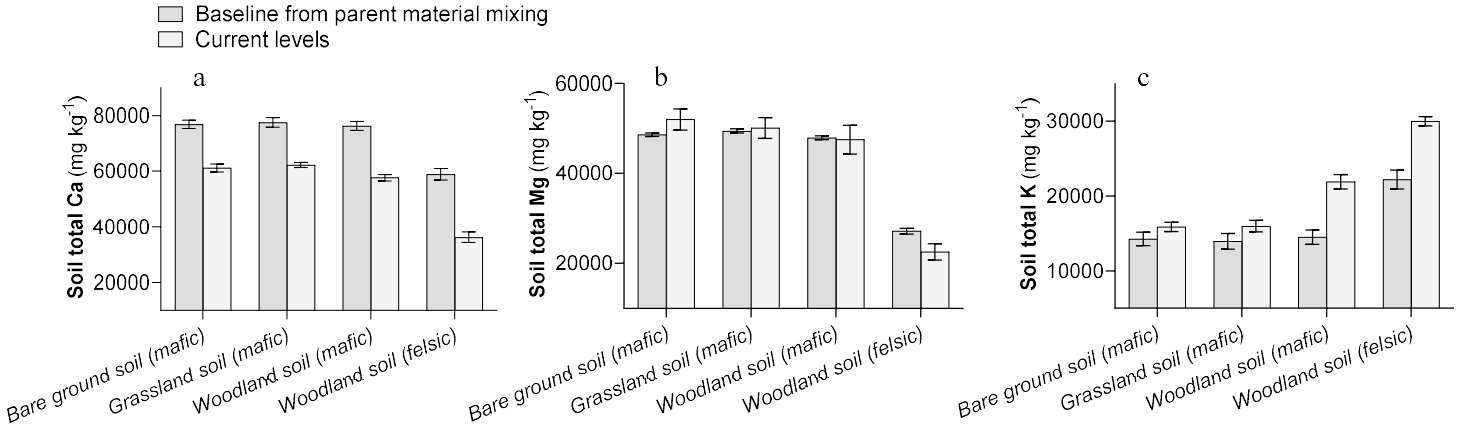

d

Oxide/ element	Chatala saponite clays	Chatala illite-smectite clays	Chatala soil exchangers
SiO_2 %	35.90 (0.45)	47.51 (2.45)	-
Al_2O_3 %	15.34 (0.24)	16.89 (1.79)	-
Fe (mg kg^{-1})	98,056 (2,730)	32,335 (14,899)	-
Mg (mg kg^{-1})	24,719 (3,509)	18,143 (8,113)	1,000 (84)
K (mg kg^{-1})	27,491 (490)	51,337 (5,011)	1,235 (486)
Ca (mg kg^{-1})	17,812 (749)	10,986 (3,417)	7,768 (1,797)

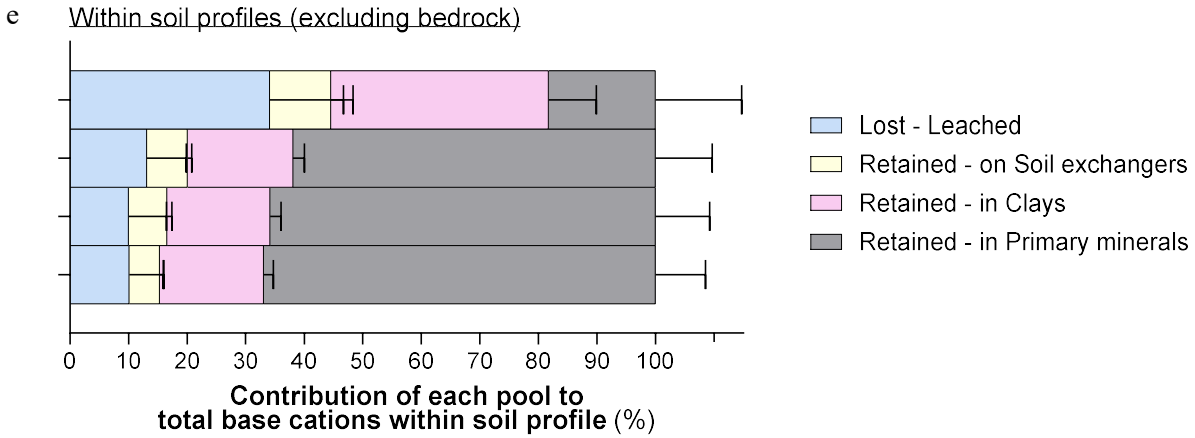

Figure 4. Cation budgets at the Chatala system – **a-c.** Comparison of major base cations (Ca, Mg, K) at baseline (calculated from parent material mixing as per Figure 3c and parent elemental concentrations – as per Figure 1d) with current levels. The difference is considered lost from the system through leaching; **d.** Major base cations on soil exchangers and incorporated into clays. The exchangers values shown here are average across the soils and these were deducted from the clays to account for exchangeable vs. structurally incorporated/immobilised cations; **e.** Breakdown of total cation pools (in equivalent molarity) into 4 pools (lost through leaching, retained on soil exchangers, retained into clays, and retained still in unweathered primary minerals). The amount in unweathered primary minerals was calculated as all other 3 pools were deducted from the current soil levels for the given cation. Note that uptake into vegetation is considered negligible and it is not taken into account.

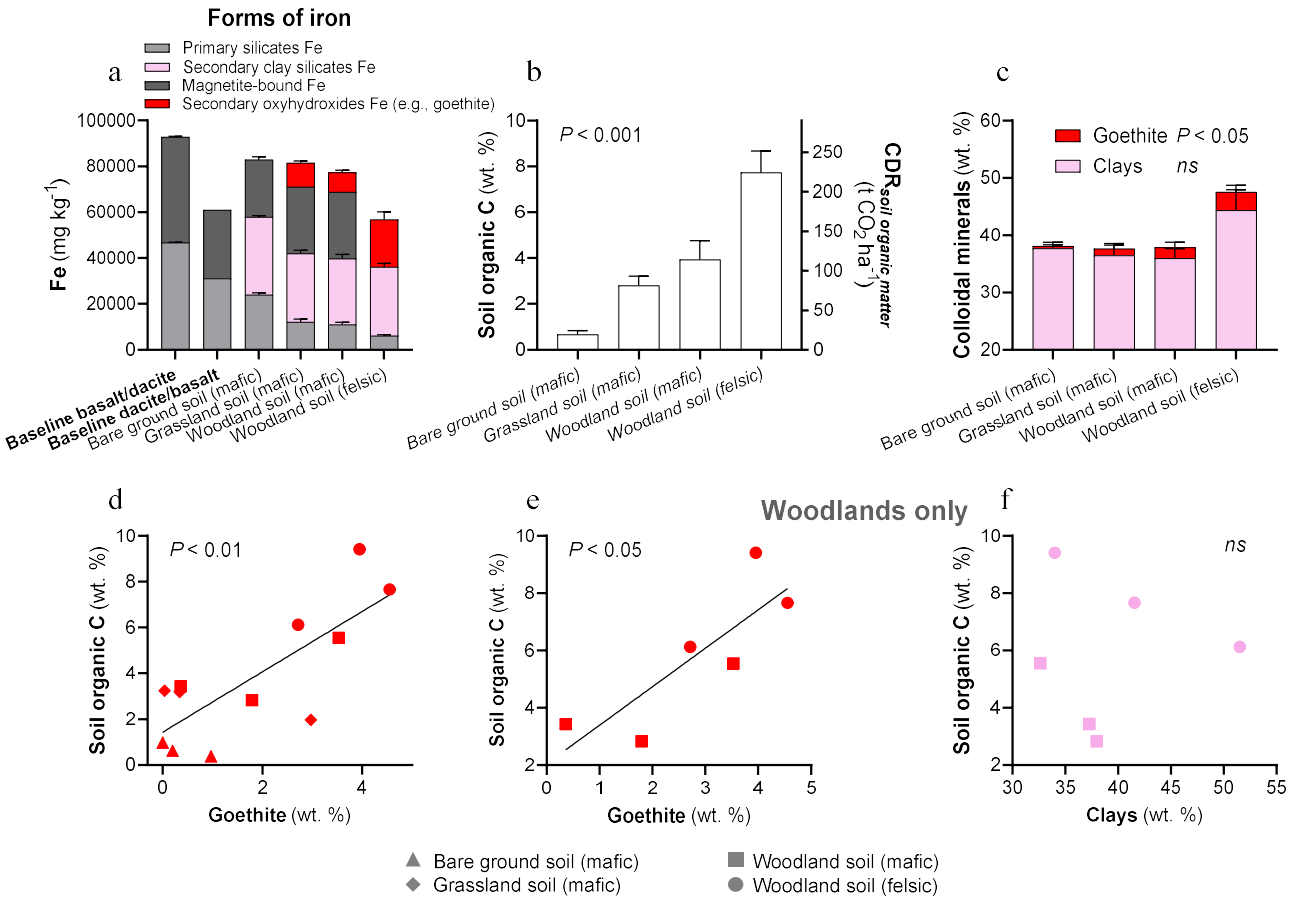

Figure 5. Iron speciation during rock weathering and the role of iron oxyhydroxides in promoting C-capture into soil organic matter through stabilisation. a. Forms of iron in each of the parent materials and soils. Note that the iron in secondary oxyhydroxides was calculated by deducting all other iron forms (using idealized mineral chemistry) from the total measured iron (as per Figure 3a); **b.** Soil organic C and CO_2 locked into soil organic matter ($CDR_{soil\ organic\ matter}$) across soils; **c.** Weight concentration of colloidal minerals (clays and goethite) across soils; Goethite here is based on mineralogical quantification – note the large similarity between these mineralogical estimates and those provided by elemental partition shown in panel a of this figure; **d.** Significant correlation of soil organic C correlation with goethite across all soils (Pearson's correlation test, $P < 0.01$); **e.** Significant correlation between soil organic C and goethite across woodland soils only (Pearson's correlation test, $P < 0.05$); **f.** Lack of significant correlation between soil organic C and clays across woodland soils (Pearson's correlation test, $P > 0.10$).

Supplementary Figures

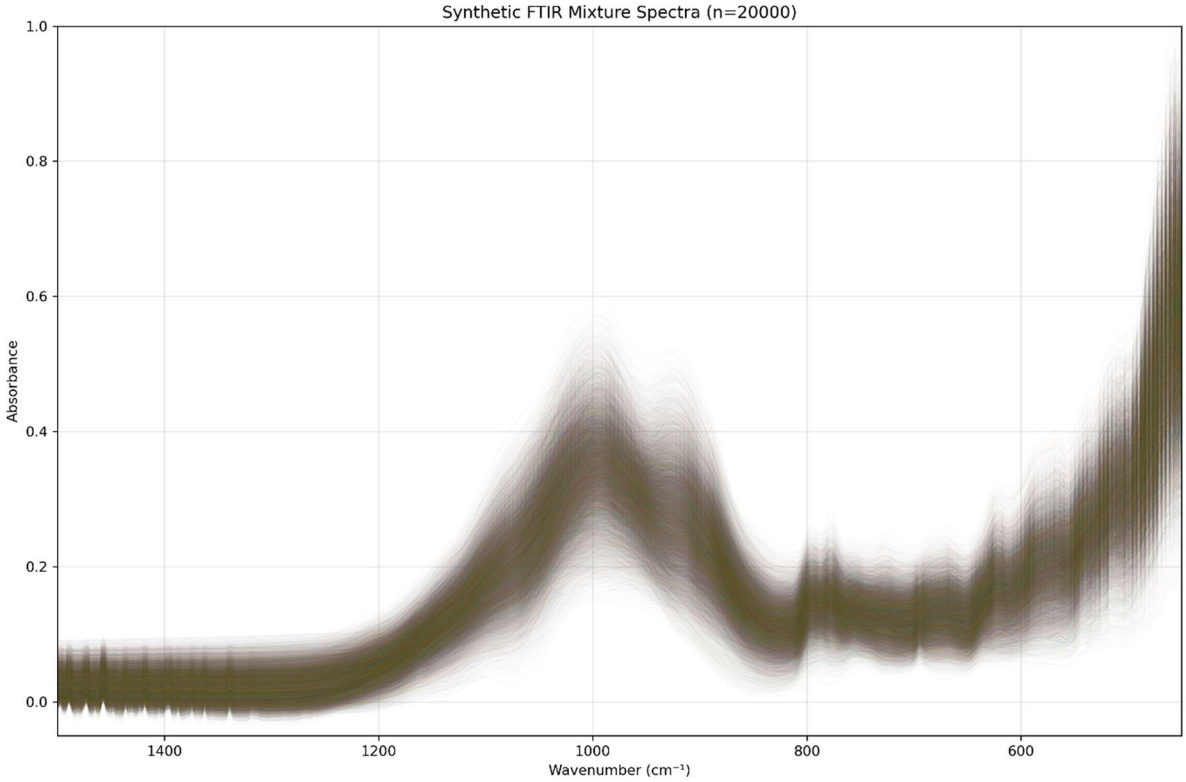

Supplementary Figure 1. Synthetic theoretical mixture spectra used for training the PLS model for predicting mineralogy in our samples. Shown is the region 1500 cm – 500 cm^{-1}.

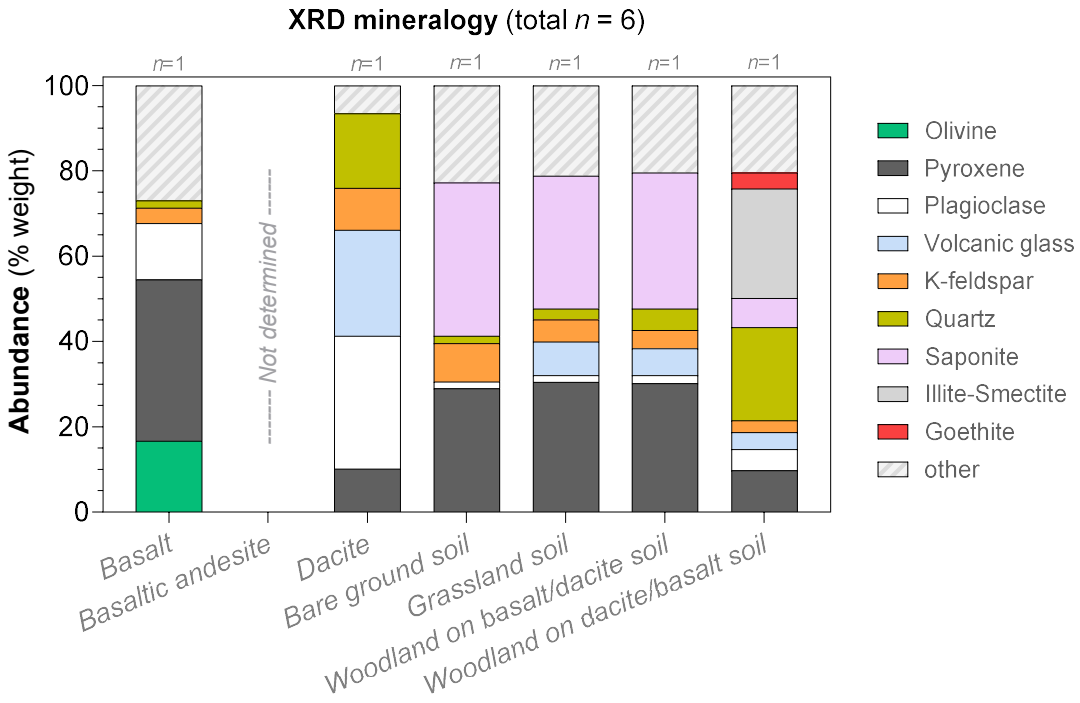

Supplementary Figure 2. XRD analyses of a selected subset of samples. These quantitative mineralogy results were used for the correlations presented in Figure 2a. Note the smaller replication (total *n*=6) relative to the total number of samples for which FTIR-PLS-based mineralogical predictions were made (total *n*=21) as presented in Figure 2b.

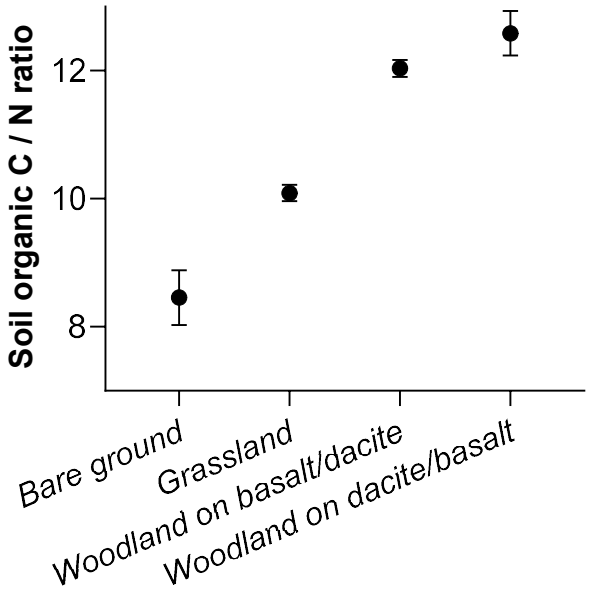

Supplementary Figure 3. Soil organic C / N analyses. Note that the C/N ratio of felsic (dacite/basalt) woodland soils and mafic (basalt/dacite) soils did not differ significantly (P>0.10) either when tested on their own through a two-tailed t-test or with group ANOVA test with post-hoc comparisons.

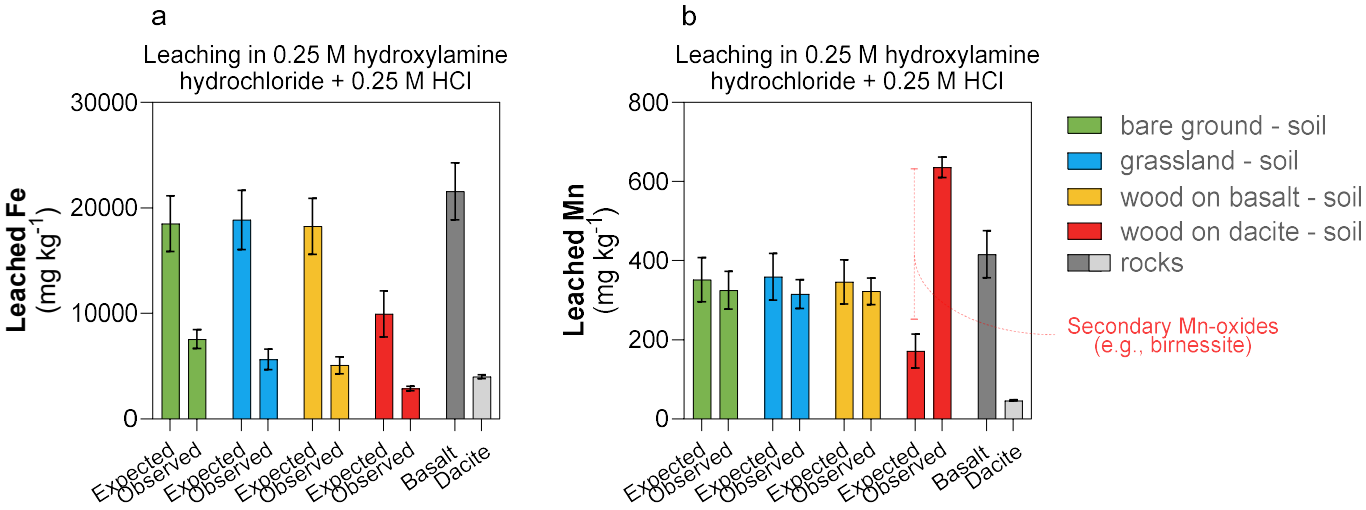

Supplementary Figure 4. Selective extractions of soil/rock. Although the extraction with 0.25 hydroxylamine hydrochloride + 0.25 M hydrochloric acid is designed to target mainly amorphous and poorly crystalline Fe oxyhydroxides (e.g., ferrihydrite) and crystalline Mn oxyhydroxides (e.g., birnessite) – it is obvious that the procedure also leaches substantial amounts of Fe and Mn even in fresh rocks where these oxyhydroxides are generally not found. Therefore, we had to calculate expected levels of leached Fe and Mn based on the leaching of their respective parent materials (basalt, dacite) and their mixing ratio. Only cases where observed is significantly higher than expected could we confidently assign the presence of these secondary oxyhydroxide mineral phases – e.g., felsic woodland soil on dacite for Mn (b). In all other cases (in both a and b panels) this was impossible with this procedure.